Title

Residential Wood Burning and Vehicle Emissions as Major Sources of Environmentally Persistent Free Radicals in Fairbanks, Alaska.

Journal

Environmental Science and Technology, 58(32)

Authors

Edwards, Kasey
Kapur, Sukriti
Fang, Ting
et al.

Publication Date

2024-08-13

DOI

10.1021/acs.est.4c01206

Peer reviewed

Environmental Science & Technology

pubs.acs.org/est

Article

Residential Wood Burning and Vehicle Emissions as Major Sources of Environmentally Persistent Free Radicals in Fairbanks, Alaska

Published as part of Environmental Science & Technology virtual special issue "Wildland Fires: Emissions, Chemistry, Contamination, Climate, and Human Health".

Kasey C. Edwards, Sukriti Kapur, Ting Fang, Meeta Cesler-Maloney, Yuhan Yang, Andrew L. Holen, Judy Wu, Ellis S. Robinson, Peter F. DeCarlo, Kerri A. Pratt, Rodney J. Weber, William R. Simpson, and Manabu Shiraiwa*

Cite This: *Environ. Sci. Technol.* 2024, 58, 14293−14305

Read Online

ACCESS | Metrics & More | Article Recommendations | Supporting Information

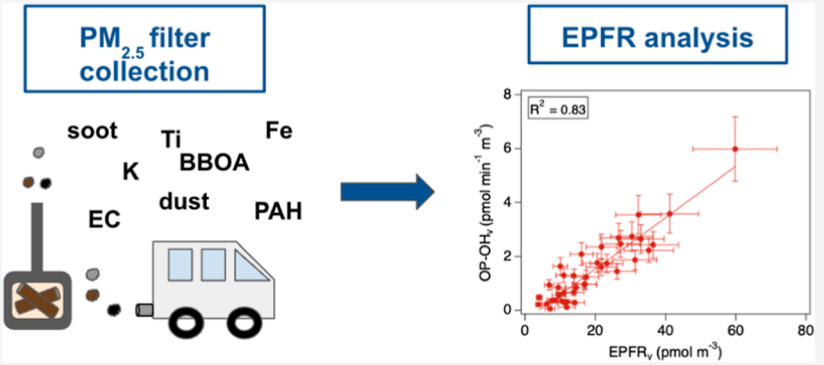

ABSTRACT: Environmentally persistent free radicals (EPFRs) play an important role in aerosol effects on air quality and public health, but their atmospheric abundance and sources are poorly understood. We measured EPFRs contained in $PM_{2.5}$ collected in Fairbanks, Alaska, in winter 2022. We find that EPFR concentrations were enhanced during surface-based inversion and correlate strongly with incomplete combustion markers, including carbon monoxide and elemental carbon ($R^2 > 0.75$). EPFRs exhibit moderately good correlations with PAHs, biomass burning organic aerosols, and potassium ($R^2 > 0.4$). We also observe strong correlations of EPFRs with hydrocarbon-like organic aerosols, Fe and Ti ($R^2 > 0.6$), and single-particle mass spectrometry measurements reveal internal mixing of PAHs, with potassium and iron. These results suggest that residential wood burning and vehicle tailpipes are major sources of EPFRs and nontailpipe emissions, such as brake wear and road dust, may contribute to the stabilization of EPFRs. Exposure to the observed EPFR concentrations (18 ± 12 pmol m^{-3}) would be equivalent to smoking ~0.4−1 cigarette daily. Very strong correlations ($R^2 > 0.8$) of EPFR with hydroxyl radical formation in surrogate lung fluid indicate that exposure to EPFRs may induce oxidative stress in the human respiratory tract.

KEYWORDS: *subarctic, free radicals, biomass burning, oxidative stress, residential heating*

1. INTRODUCTION

Environmentally persistent free radicals (EPFRs) are pollutants of growing concern that are contained within atmospheric particulate matter (PM).[1−4] EPFRs are primarily formed from incomplete combustion, including biomass burning, vehicle exhaust, and coal combustion.[2,3,5−9] Previous studies have found that EPFR concentrations were positively correlated to $PM_{2.5}$, NO_2, and CO—common byproducts of coal combustion, biomass burning, heating oil, and automobile emissions.[10−14] In contrast to other short-lived radicals in the atmosphere, EPFRs have much longer lifetimes from minutes to over hours and days to no decay in the atmosphere.[10,15,16] Because of their long lifetimes, EPFRs can undergo long-range transport. Previous studies have observed regional and seasonal variations in EPFR concentrations.[10,17,18] One useful metric to determine relative air quality risk in different regions is to compare the EPFR concentration found within PM to the concentration of free radicals found within cigarettes.[11,12,15]

Received: February 1, 2024
Revised: July 17, 2024
Accepted: July 18, 2024
Published: August 2, 2024

The first study using this metric found that nonextreme air quality risk in the US has EPFR concentrations equivalent to smoking 0.4−0.9 cigarettes per day.[15] In addition, EPFRs are redox active and induce the formation of reactive oxygen species (ROS) in the aqueous phase; hence, inhalation and respiratory deposition of EPFRs may cause oxidative stress and adverse health effects.[1,19−22]

Electron paramagnetic resonance (EPR) spectroscopy can be used to detect and quantify EPFRs. EPFRs are formed in postflame combustion in which aromatic products adsorb to metal oxides which stabilize and catalyze EPFR production through surface-mediated reactions.[8,9,23−26] Identifying metals associated with EPFRs can help to determine sources of EPFR, as some metals are good tracers for specific emission source. Visible light and solar-simulated irradiation has been shown to catalyze EPFR production from soot particles and polycyclic aromatic hydrocarbons (PAHs),[27−29] but we expect this process is diminished with limited UV and visible irradiation in winter in Fairbanks.

Fairbanks, Alaska, has a subarctic climate with very low temperatures and short daylight hours in winter. Due to a net heat loss from the surface, Fairbanks often experiences temperature inversions in winter, amounting to 60−80% of days.[30,31] The surrounding mountains block wind to the Fairbanks basin, preventing mixing and dilution, which leads to the trapping and stagnation of polluted air with high levels of PM and other pollutants in a shallow boundary layer.[30,32−34] As a result, Fairbanks often exceeds the daily National Ambient Air Quality Standard for $PM_{2.5}$ (35 $\mu g\ m^{-3}$) in the winter.[35] Source apportionment studies have shown that wood smoke and sulfate from sulfur-containing fuel combustion are dominant sources of $PM_{2.5}$, followed by gasoline and diesel emissions.[36,37] A recent study has confirmed that wood burning is a significant contributor to $PM_{2.5}$ emissions in Fairbanks during the winter of 2022.[38] Due to the increased residential heating from wood and pellet residential stoves in the winter, heightened levels of EPFRs are expected, but EPFRs have never been measured in Fairbanks.

The Alaskan Layered Pollution And Chemical Analysis (ALPACA) Campaign was conducted in Fairbanks, Alaska during January to February 2022 to study wintertime subarctic atmospheric chemistry and meteorology.[39] The purpose of this study is to quantify EPFRs over this period and to assess their impact on the toxicological risk of inhalation of ambient wintertime air. Using a $PM_{2.5}$ high volume sampler, we collected filter samples for detection and quantification of EPFRs offline by EPR spectroscopy. We assess the relationship between EPFRs and atmospheric gases, metals, and particulate pollutants. By comparing our results with previous studies in other environments, we aim to elucidate the impact of cold and dark environments and meteorology on the EPFR concentration. We also quantify the cigarette equivalence and the relationship between EPFRs and hydroxyl radical formation in surrogate lung fluid to assess the health implications of EPFRs and their ability to induce oxidative stress.

2. MATERIALS AND METHODS

2.1. $PM_{2.5}$ Collection. A $PM_{2.5}$ high-volume sampler (Tisch Environmental) was used to collect ambient $PM_{2.5}$ at a suburban house site in Fairbanks, Alaska (64.8502N, −147.6755°E). Samples were collected for 23.5 h each day from 01/16/2022 to 2/25/2022. The measured flow rate fluctuated within 12% of the set flow rate of 40 cubic feet min^{-1}. Samples were collected onto a prebaked quartz filter size 8 in. × 11 in. with a particle collection area of 7 in. × 9 in. Filters were immediately wrapped in prebaked aluminum foil, sealed, and then stored in the freezer (−18 °C) until analysis with the exception of a two day period where filters were transported in a cooler with ice packs from Fairbanks, AK to Irvine, CA for analysis. Blank filters were collected once per week by having them go through a normal sample preparation and placing in the high-volume sampler for 30 s without air flow without $PM_{2.5}$ collection followed by storage procedure.

2.2. Environmentally Persistent Free Radicals (EPFRs). The high-volume filters were analyzed for EPFRs within 2 months of the time of collection by using an X-band continuous-wave EPR spectrometer (Bruker, Germany). A circular punch with a diameter of 1.0 in. was taken from each high-volume filter for EPFR analysis. The EPFR concentrations were quantified using a calibration curve of TEMPOL, 4-Hydroxy-2,2,6,6-tetramethylpiperidine-1-oxyl (Sigma-Aldrich), with a calibration range of 1.1−220 μM (Figure S1). The parameters for EPFR measurements were as follows: attenuation of 10 dB, a modulation amplitude of 3.0 G, microwave power of 20.00 mW, and a receiver gain of 40 dB. For EPFR analysis, the filter was placed into a quartz tube (9.17 mm I.D., SP Wilmad-LabGlass) and then directly placed in the resonator. The samples were scanned over the field range of 3300−3700 G and averaged over 5 scans. Sample stability was investigated by analyzing the filters again 6 months after collection (Figure S4). Two replicates were taken using different filter punches from four different sample dates. The error was calculated to be ∼15% for those sampling dates and assumed to be the percent error for all sampling dates. Daily concentrations are presented as EPFRs per volume of air ($EPFR_v$, pmol m^{-3}) and per mass of $PM_{2.5}$ ($EPFR_m$, pmol μg^{-1}). $EPFR_v$ is relevant for addressing human exposure and public health concerns, as people breathe in air by volume. $EPFR_m$ represents the relative contribution of EPFRs to particles, which is indicative of the intrinsic toxicity of PM. Thus, it is more reasonable to conduct correlation analysis for $EPFR_v$ with ambient concentrations of various pollutants (correlations of $EPFR_m$ are included in SI for completeness). We applied an ANOVA test to obtain the p-values, and the determination coefficient R^2 was calculated using Pearson's correlation coefficient R calculated in Igor Pro to evaluate the strength of correlation.[40]

Following Gehling and Dellinger[15] and Chen et al.,[11] we calculated the equivalent amount of cigarettes per day (EQ) using the equation below.

$$EQ = \frac{RI}{RC_{cig}C_{tar}} \quad (1)$$

The amount of radicals inhaled with $PM_{2.5}$ is calculated as RI (pmol/day). RC_{cig} is the radical spins in a gram of tar, which was reported to be 1.75×10^{16} radicals/g (0.0291 pmol μg^{-1}) by Gehling and Dellinger[15] and 4.75×10^{16} radicals/g (0.0789 pmol μg^{-1}) by Chen et al.[11] Both values were used to calculate minimum and maximum estimations for equivalent cigarette smoking. C_{tar} is the average mass of tar found per cigarette (0.013 g), based on previous studies.[11,15] RI can be calculated as below

$$RI = EPFR_v V = EPFR_m C_{PM} V \quad (2)$$

https://doi.org/10.1021/acs.est.4c01206
Environ. Sci. Technol. 2024, 58, 14293−14305

where V is the breathed air volume as assumed to be 20 m^3 per day and C_{PM} is the measured mass concentration of $PM_{2.5}$ ($\mu g\ m^{-3}$).

2.3. Mass Concentrations of PM Composition. To determine the organic carbon (OC) and elemental carbon (EC) in $PM_{2.5}$ in Fairbanks, a 1.5 cm^2 filter punch from the high volume filters was analyzed by a Sunset OC/EC analyzer (Sunset Laboratory Inc. OR, USA) using the National Institute for Occupational Safety and Health (NIOSH) 5040 analysis protocol.[41] Total carbon (TC) is the sum of OC and EC. Mass concentrations of daily $PM_{2.5}$ ($\mu g\ m^{-3}$) were estimated through summation of elemental carbon and nonrefractory sulfate, nitrate, organics, and chlorine as measured by the AMS. Note that AMS measures PM_1 without dust and salt (i.e., refractory species), which may lead to an underestimation of $PM_{2.5}$. The absolute difference between the calculated $PM_{2.5}$ and a $PM_{2.5}$ monitor located 800 m WSW of the house site Fairbanks was ~25%.

Polycyclic aromatic hydrocarbons (PAHs), hydrocarbon-like organic aerosols (HOA), and biomass burning organic aerosols (BBOA) data were obtained from the High-Resolution Time-of-Flight Aerosol Mass Spectrometer (HR-ToF-AMS) data collected from PM_1 at the house site in Fairbanks (64.8502N, −147.6755°E). A three-factor positive matrix factorization analysis of the mass spectra yielded HOA, BBOA, and PAH factors. Two distinct OA mass spectral factor profiles that best describe the variability in the OA matrix were identified using PMF based on the method described by Ulbrich et al.[42] We label these profiles as BBOA and HOA. We named each factor based on (1) similarity to previously published factor profiles, which we downloaded from the AMS spectral database (https://cires1.colorado.edu/jimenez-group/AMSsd/), and (2) expected diurnal behavior, as discussed below in the subsequent subsection.[43] The PAH factor was determined using the method based on a modification of the standard AMS "fragmentation table," which was developed from fragmentation patterns from laboratory standards of different aerosolized PAHs.[44] While this method does not speciate the PAHs, PAH are (relatively) resistant to fragmentation, and so are easier to identify at larger m/z ratios.[45] We did not observe strong correlations between the PAH concentration and the AMS PMF factors that would be indicative of a single emissions source.

2.4. Gaseous Pollutants and Temperature Measurements. SO_2, CO, O_3, NO_x, and temperature data were monitored at a downtown location (64.8411N, −147.7275°E) in Fairbanks which was 2 miles away from the house site. SO_2 was measured using a Thermo 43C Pulsed fluorescence SO_2 analyzer. CO was measured using a Thermo 48C gas filter correlation CO analyzer. NO_x was measured by using a Thermo 42C Chemiluminescence $NO-NO_2-NO_x$ analyzer. O_3 was measured using a Thermo 49C UV photometric O_3 analyzer. All gases, except CO_2, were calibrated roughly weekly using EPA certified standard gases and an O_3 generator to react O_3 with NO when calibrating the NO_x analyzer. Temperature probes at heights of 23 and 3 m were placed at the downtown site. Temperature probes were made of thermistors inside metal sealed with epoxy, and calibrated using the method described in Cesler-Maloney et al.[34] They were deployed as functioned aspirated thermometers with a fan keeping airflow constant around the probes. Number of hours under inversion was calculated by adding all hours of the day that experienced a temperature inversion, $dT = T$ at 23 m − T at 3 m greater than 0.5 °C.

2.5. ICP−MS Analysis of $PM_{2.5}$. To measure the total concentration of metals, one 1.5 cm^2 filter punch from the high volume filter was acid-digested using aqua regia (HNO_3 + 3HCl). The filter was incubated in the acid at 99 °C and shaken at a rotational frequency of 400 rpm using a ThermoMixer instrument (Eppendorf North America, Inc., Hauppauge, NY, USA) for 24 h. The acid-digested sample was then diluted in DI to a final nitric acid concentration of 2% (v/v) and filtered through a 0.45 μm PTFE syringe filter.[46] The metals were analyzed by inductively coupled plasma mass spectrometry (ICP−MS, Agilent 7500a series, Agilent Technologies, Inc., CA, USA) following EPA method 6020 (EPA, 2014).[47] We measured concentrations of various elements including magnesium, aluminum, potassium, titanium, manganese, iron, nickel, copper, zinc, molybdenum, antimony, and lead. Limits of detection are listed in Table S1.

2.6. Online Single-Particle Analysis. Real-time measurements of the size and chemical composition of 627,088 individual aerosol particles with vacuum aerodynamic diameter (d_{va}) of 0.1−1.0 μm were characterized using an aerosol time-of-flight mass spectrometer (ATOFMS) based on the design of Pratt et al.[48] and described by Gunsch et al.[49] Individual particle dual-polarity mass spectra were imported into MATLAB (Mathworks) and analyzed using FATES, a custom analysis toolkit.[50] An adaptive resonance theory-based clustering method (Art-2a)[51] with a vigilance factor of 0.65 and learning rate of 0.05 for 20 iterations was used to group similar single-particle mass spectra into clusters, which were then used to identify individual particle sources, which will be described in a forthcoming manuscript. For the work herein, single-particle mass spectra were then searched for specific ions of interest. Iron-containing particles were identified using a peak area ratio of the two most abundant isotopes of iron (^{56}Fe and ^{54}Fe) between 8 and 32 [half to twice the natural isotopic ratio (16)];[52,53] this criterion resulted in 5123 individual iron-containing particles. PAHs were then identified in iron-containing particles by the detection of molecular ions of several PAHs,[54−56] including naphthalene [m/z 128 ($C_{10}H_8^+$)], acenaphthylene [m/z 152 ($C_{12}H_8^+$)], phenanthrene/anthracene [m/z 178 ($C_{14}H_{10}^+$)], pyrene/fluoranthene [m/z 202 ($C_{16}H_{10}^+$)], chrysene/benzanthracene/benzophenanthrene/triphenylene [m/z 228 ($C_{18}H_{12}^+$)], and benzopyrene/benzofluoranthene/perylene [m/z 252 ($C_{20}H_{12}^+$)]. These searches resulted in 3109 individual particles being identified as containing both iron and PAHs. Additional description of trace metal- and PAH-containing particles will be the focus of future manuscripts.

2.7. Hydroxyl Radical Oxidative Potential (OP^{OH}) Assay. The high-volume $PM_{2.5}$ filters were analyzed for OP by OH production in a synthetic lung fluid assay (OP^{OH}). A fraction from each filter was placed in a sterile polypropylene centrifuge vial (VWR International LLC, Suwanee, GA, USA). Due to the possible nonlinear response of OP end points with extract mass concentration,[57] the punched filter fraction and the volume of water used for extraction were determined based on the $PM_{2.5}$ mass loading on each filter to achieve a relatively constant sample concentration 25 $\mu g\ mL^{-1}$ for OP^{OH} analysis in the reaction vial. Filters were extracted in deionized Milli-Q water (DI, Nanopure InfinityTM ultrapure water system; resistivity >18 MΩ/cm) via 60 min sonication (Ultrasonic Cleanser, VWR International LLC, West Chester, PA, USA).

https://doi.org/10.1021/acs.est.4c01206
Environ. Sci. Technol. 2024, 58, 14293−14305

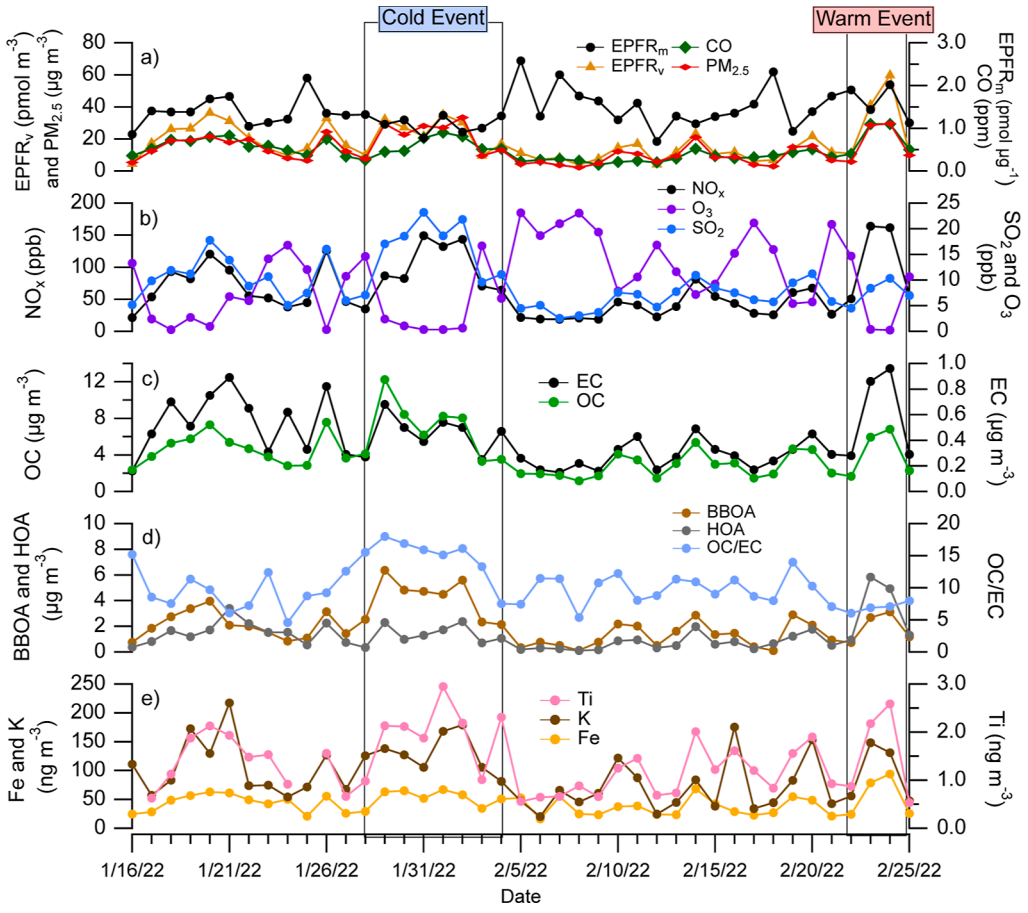

Figure 1. Daily concentrations of EPFR$_v$, EPFR$_m$, NO$_x$, SO$_2$, O$_3$, OC, EC, BBOA, HOA, and selected metals (Fe, K, and Ti) during the ALPACA campaign. The gray boxes highlight the cold and warm pollution events during the campaign. Trace gas data has been reported as the averaged value over the EPFR sampling period.

The PM extracts were not filtered, and the filter punch was left in the extracts throughout the OP analysis so insoluble species could be in contact with the reagents.[58] Established protocols were used for the OP^{OH} methods,[59] with details given in the Supporting Information. OP$_v^{OH}$ is normalized by the volume of air sampled (pmol min^{-1} m^{-3}).

3. RESULTS AND DISCUSSION

3.1. Characterization and Time Series of EPFR. Figure 1a shows concentrations of EPFRs per air volume (EPFR$_v$) and PM$_{2.5}$ mass (EPFR$_m$). A typical EPFR spectrum is shown in Figure S2. The average *g*-factor of EPR signals for the course of the campaign was 2.0021 ± 0.0001. *G*-factors of <2.003 and 2.003−2.004 are indicative of carbon-centered and oxygen-centered radicals, respectively.[3,10,24,26] EPFRs observed in urban air, with emissions from fossil fuels, industry, and vehicles, often have *g*-factors ranging from 2.0027 to 2.0037.[3,18,60] The observed average *g*-factor in Fairbanks is lower, but similar to the range of *g*-factors found in other areas that have a significant traffic contribution such as Beijing,[5] Xi'an,[11] and Fujian[61] with a *g*-factor of 2.0031−2.0038 and Southern California highway sites with 2.0020−2.0032.[62,63] Another study observed a similar *g*-factor of 2.0022 for EPFRs associated with traffic emissions.[10] The peak-to-peak distance ($\Delta H_{p\text{-}p}$), which can provide an insight on the type of EPFR species,[8] was found to be 6 ± 1 G, which is similar to EPFR signals found in China,[11] Germany,[18] Pakistan,[17] and California.[62]

The EPFR concentration per meter cubed of air sampled (EPFR$_v$) in Fairbanks ranged from 5 to 60 pmol m^{-3} with average concentration of 18 ± 12 pmol m^{-3}. The average EPFR$_v$ in Fairbanks is higher than a suburban site in Irvine (14 ± 12 pmol m^{-3} for PM$_{2.5}$) and downwind of a wildfire site (8 ± 8 pmol m^{-3} for PM$_{10}$),[62,63] but lower than EPFR$_v$ near a highway site in Southern California (36 ± 14 pmol m^{-3} for PM$_{2.5}$).[62,63] Note that actual ambient EPFR concentrations in Fairbanks may be higher than our measured value because EPFR analysis was completed 1−2 months after collection as opposed to within 2 weeks for the near highway study.[62] EPFR$_v$ for the warmer urban climate of Xi'an, China was much higher than Fairbanks, with a concentration ranging from 73 to 1154 pmol m^{-3} in the winter (range of 4.44 × 10^{13} to 6.95 × 10^{14} spins m^{-3}).[11] The winter EPFR$_v$ for Lahore, Pakistan was also higher than Fairbanks, with a concentration of 48−480 pmol m^{-3}.[17] This may be due to the fact that PM$_{2.5}$ concentrations were also much higher in Xi'an (28−490 μg m^{-3}) and Lahore (522.2 ± 222.0 μg m^{-3}) compared to Fairbanks (2−33 μg m^{-3}).[11,17]

The average EPFR concentration per microgram of PM$_{2.5}$ (EPFR$_m$) was 1.4 ± 0.4 pmol μg^{-1}. If we assume the average EPFR molecule has a MW of 200 g mol^{-1} (assuming that EPFRs are similar to anthraquinone), we find that ∼0.03% of PM$_{2.5}$ mass would be attributed to EPFRs. EPFR$_m$ in Fairbanks is higher than EPFR$_m$ measured in other cities including

https://doi.org/10.1021/acs.est.4c01206
Environ. Sci. Technol. 2024, 58, 14293−14305

Table 1. Average $EPFR_v$ (pmol m^{-3}), $EPFR_m$ (pmol μg^{-1}), EPFR-Equivalent Cigarettes per Day, and *g*-Factor Values of EPR Spectra for PM Collected in Fairbanks (This Study), in Comparison to Previous Measurements at Highway Sites in Southern California (Hwang et al., 2021),[62] Irvine, CA (Hwang et al., 2021),[62] Downstream of a Wildfire (Fang et al., 2023),[63] Xi'an (Chen et al., 2019),[11] Beijing (Yang et Al., 2017),[5] Linfen (Chen et Al., 2020),[65] Mainz (Arangio et al., 2016; Filippi et al., 2022),[18,64] and Lahore (Ahmad et al. 2023)[17a]

	$EPFR_v$ (pmol m^{-3})	$EPFR_m$ (pmol μg^{-1})	average cigarettes per day	g-factor
Fairbanks (winter), AK	18 ± 12	1.4 ± 0.4	0.4−1.0	2.0021 ± 0.0001
Highway, CA	36 ± 14	2.5 ± 2.0[b]	0.7−1.9[b]	2.0027 ± 0.0001
Irvine (suburban), CA	14 ± 12	N/A	0.3−0.7[b]	N/A
Wildfire, CA (PM_1)	2.9−7.6	0.6 ± 0.4	0.1−0.4[b]	2.0028 ± 0.0003
Xi'an, China (winter)	349[b]	N/A	6.8−18.5[b]	2.0035 ± 0.0003
Beijing (haze), China (PM_1)	5.11×10^4[b]	N/A	996−2,700[b]	2.0032−2.0037
Linfen (winter), China ($PM_{2.1}$)	300−600[b]	N/A	6−32[b]	2.0034−2.0037
Mainz, Germany (PM_{TSP})	6.0 ± 5.3[b]	0.7 ± 0.1	0.1−0.3[b]	∼2.003
Lahore (winter), Pakistan	200 ± 120[b]	0.4 ± 0.1[b]	3.9−10.6	2.0027−2.0032

[a]Cigarettes per day value is originally reported value unless otherwise stated. [b]Indicates an estimated value based on reported results. $PM_{2.5}$ values unless otherwise specified. PM_{TSP} is the measurement of total suspended particles.

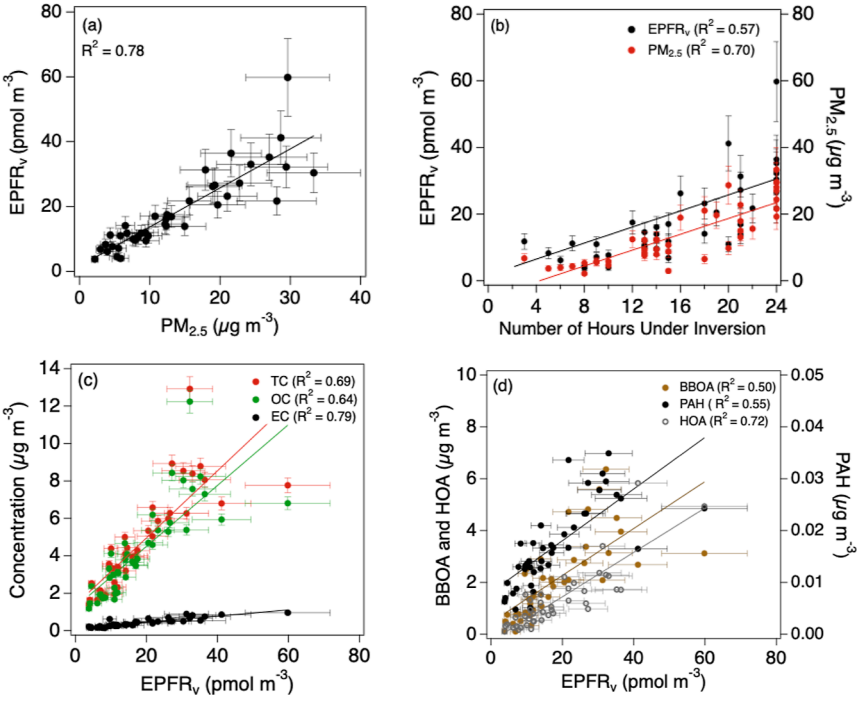

Figure 2. (a) Correlation between $PM_{2.5}$ and $EPFR_v$ concentrations. (b) $EPFR_v$ (black) and $PM_{2.5}$ (red) plotted against the daily inversion time (out of 24 h). (c) Correlations of $EPFR_v$ (pmol m^{-3}) with mass concentrations (in $\mu g\ m^{-3}$) of total carbon (TC-red), organic carbon (OC-green), and elemental carbon (EC-black). (d) Correlations between $EPFR_v$ and mass concentrations (in $\mu g\ m^{-3}$) of polycyclic aromatic hydrocarbons (PAH-black), biomass burning organic aerosols (BBOA-brown), and hydrocarbon-like organic aerosols (HOA-gray). All correlations shown in (a−d) have *p*-values <0.001.

Mainz, Germany,[18,64] Lahore, Pakistan[17] and Irvine, CA, during wildfires,[63] but lower than measurements next to the highway, as shown in Table 1.[62]

Figure 1 shows the time series of EPFR and gaseous pollutants including CO, NO_x, SO_2, and O_3 as well as particulate pollutants including EC, OC, BBOA and HOA. Selected metals are also shown as tracers for biomass burning (K) and nontailpipe emissions (Fe, Ti) including brake wear and road dust (see Section 3.4). There were two noteworthy pollution events during the campaign, characterized by high levels of $PM_{2.5}$ with ∼30 $\mu g\ m^{-3}$. The first event was from Jan 29 to Feb 3, 2022, which was a "cold event" in which temperatures averaged from −35 to −16 °C with a major emission source of residential wood burning.[39] The second event was characterized as a "warm event" in which temperature ranged from −12 to 2 °C during Feb 23−25, 2022, with enhanced vehicle emissions.[39] During both events, we observed a heightened concentration of EPFRs with 31 and 60 pmol m^{-3} during the cold and warm events, respectively. The extent of enhancement of $EPFR_v$ is more prominent during the warm event compared with the cold event. This is most likely because the yield of EPFR generation by biomass burning is lower compared to vehicle tailpipes, as shown in previous studies.[62,63]

3.2. Correlation of PM Components with EPFR. One important component of air pollution is $PM_{2.5}$. Figure 2a shows that $EPFR_v$ and $PM_{2.5}$ have a strong correlation with R^2 = 0.78. Surface-based temperature inversion, which often

https://doi.org/10.1021/acs.est.4c01206
Environ. Sci. Technol. 2024, 58, 14293−14305

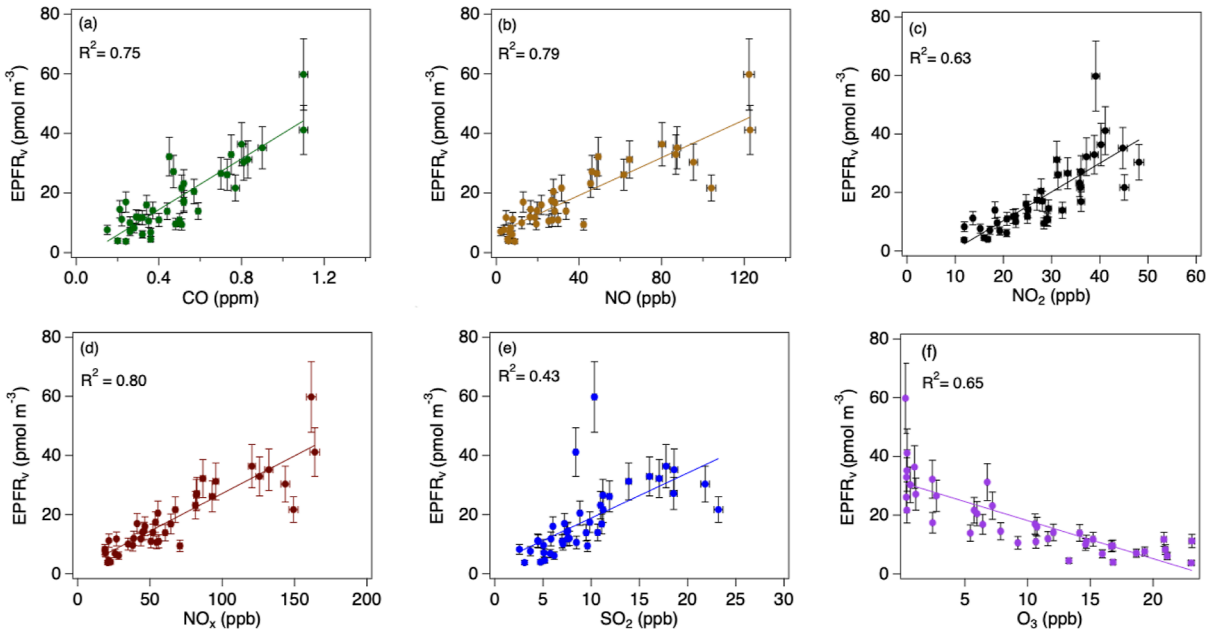

Figure 3. Correlation plots between daily average concentrations of $EPFR_v$ (pmol m^{-3}) with mixing ratios of gaseous pollutants including CO, NO, NO_2, NO_x, SO_2, and O_3. All correlations shown in Figure (a–f) have p-value < 0.01.

occurs under dark and cold conditions in winter in Fairbanks, traps air pollutants in a shallow boundary layer.[30,34] We characterized surface inversion by the number of hours in a day that had a temperature difference (dT) of >0.5 °C for dT = T at 23 m − T at 3 m at a downtown site in Fairbanks. A day during the campaign was in a surface-based inversion for an average of 16 ± 6 h. As shown in Figure 2b, we observed that both $EPFR_v$ and $PM_{2.5}$ concentrations correlate moderately with the number of hours under surface-based inversion with R^2 > 0.5. These correlations illustrate that surface inversion controls the atmospheric concentrations of EPFR and $PM_{2.5}$. There is no obvious influence of temperature or relative humidity on $EPFR_v$ (Figure S3).

As $PM_{2.5}$ is strongly correlated with EPFR, the source apportionment of $PM_{2.5}$ may provide useful insight for the source of EPFRs. Previous long-term source apportionment studies for winter in Fairbanks have found that wood smoke (20–80%), vehicle emissions (10–30%), and sulfate (10–35%) are leading contributors to $PM_{2.5}$ with minor contributions from soil and road salt (both <4%) in winter in Fairbanks.[33,36,37,66] This explains a strong correlation of $EPFR_v$ with $PM_{2.5}$ as wood smoke and vehicles can be source of EPFRs, while sulfate does not contribute to EPFR generation.[26]

EC and OC can be both generated from combustion, including biomass burning, gasoline, and diesel combustion.[33,67−69] EC is often used synonymously with black carbon or soot, and is used as a tracer for diesel exhaust emissions.[41,70,71] The observed OC is dominant from primary emissions, most likely from residential wood or pellet stoves. The OC/EC ratio can provide insights on the main combustion source as it varies based on the type of combustion: coal (0.3–13.5), diesel exhaust (0.2–0.9), gasoline exhaust (1.1–3.6), and biomass burning (4.1–15.5; up to 40 for wood combustion).[17,68,72] The OC/EC ratio in Fairbanks ranged from 4.5 to 18 with an average of 10 ± 3. Coal combustion pollution from power plants is expected to be minor in Fairbanks, as high stack heights are employed to limit ground-level pollution.[39] Wood combustion, used in residential heating, is thought to be the major combustion type. During the cold event, OC/EC reaches a peak with values above 15 (Figure 1c). The heightened OC/EC is expected as more people use their wood or pellet stoves for residential heating under very low temperatures. The AMS-derived BBOA factor indeed shows its highest concentration during the cold event (Figure 1d). Potential additional sources of OC include cooking and oxidation of volatile organic compounds, but they are unlikely to drive the higher OC/EC ratio observed here.[67] During the warm event, the OC/EC value decreases below 8.0, indicating a substantial contribution of vehicle emissions, as also shown by enhanced concentration of HOA (Figure 1d).

Figure 2c shows the correlations of $EPFR_v$ with mass concentrations of EC, OC, and total carbon (TC), exhibiting tight correlations. The correlation of $EPFR_v$ with EC (R^2 = 0.79) is stronger than $PM_{2.5}$ and all other pollutants (aside from NO_2, see section below), indicating that EPFRs in Fairbanks are indeed formed by incomplete combustion. Positive correlations of EPFRs with EC have also been observed in Xi'an[11] and at a highway site in southern California.[62] As shown in Figure 2d, $EPFR_v$ exhibits a strong correlation with BBOA (R^2 = 0.50), suggesting that residential wood burning is the major source of EPFR. $EPFR_v$ also has a strong correlation with HOA (R^2 = 0.72). HOA serves as a proxy from primary OA associated with traffic emissions.[73−75] $EPFR_v$ showed its highest value during the warm event when HOA peaked (Figure 1a), implying that vehicle emissions produce EPFRs in a higher yield than wood burning, which is consistent with a recent study.[76] HOA was also slightly enhanced during the cold event, which may imply that HOA was also emitted by residential oil heating or that there may be an increase of vehicle emissions in colder temperatures as shown by previous studies.[77,78] Note that BBOA emissions were far more enhanced than those of HOA during the cold event, suggesting that BBOA plays a more significant role during this period. We also observe a strong correlation between $EPFR_v$ and PAH (R^2 = 0.55). PAHs are often

https://doi.org/10.1021/acs.est.4c01206
Environ. Sci. Technol. 2024, 58, 14293−14305

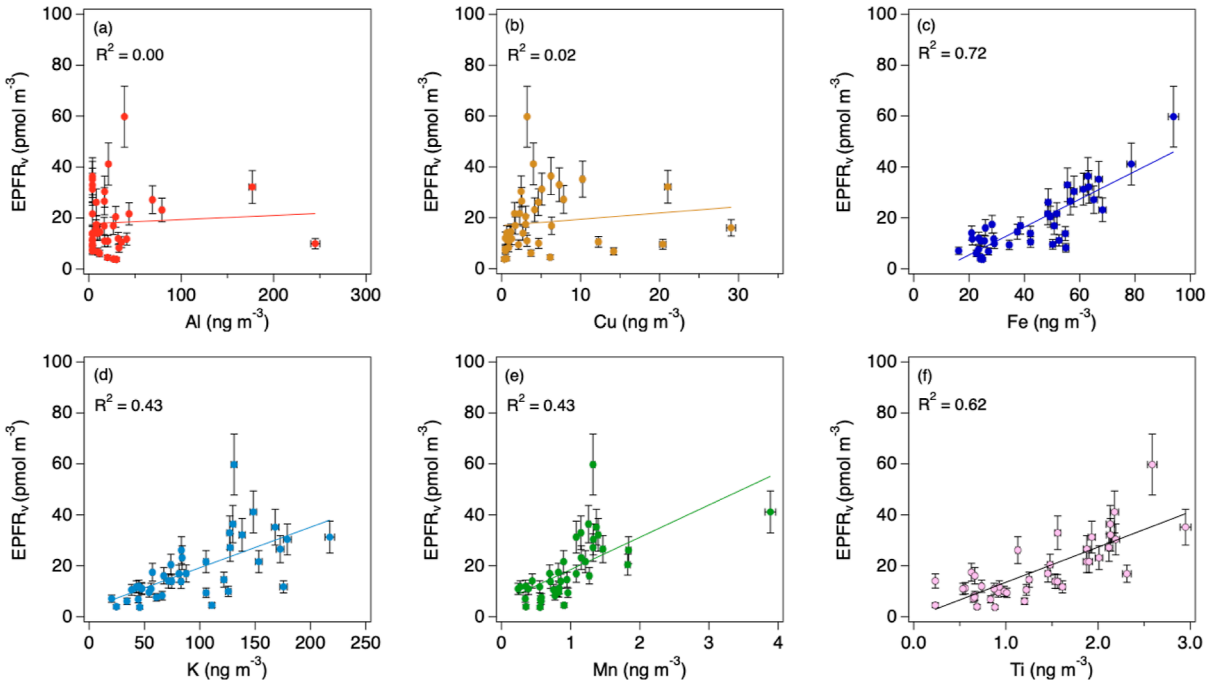

Figure 4. Correlations between daily average concentrations of $EPFR_v$ (pmol m^{-3}) with metal species (Al, Cu, Fe, K, Mn, and Ti). Correlations of EPFRs with Al and Cu have p-value >0.05. Correlations of EPFRs with Fe, K, Mn, and Ti and p-value <0.01.

associated with soot particles that can be emitted by both diesel vehicles and biomass burning.[79−82] Hence, our correlation analysis implies that EPFRs are emitted by both residential wood stoves, especially during the cold event, and vehicles, dominantly during the warm event.

3.3. Correlation of Gaseous Pollutants with EPFRs. Figure 3 shows correlation plots for $EPFR_v$ with various gaseous pollutants. CO was observed to correlate strongly with EPFRs (R^2 = 0.75), which is consistent with EPFRs being associated with incomplete combustion, as discussed above. While both NO and NO_2 correlate well with $EPFR_v$, the strongest correlation was observed between NO_x and $EPFR_v$ (R^2 = 0.80), which is expected as NO_x is emitted by wood burning and vehicles.[83,84] SO_2 was observed to correlate moderately with $EPFR_v$ (R^2 = 0.43) as shown in Figure 3e. In Fairbanks, SO_2 is emitted from fossil fuel combustion in a power plant as well as indoor heating by fuel oil. The main source of SO_2 near ground level is residential oil heating,[85] as the plume from the power plant is injected above the inversion layer and does not significantly contribute to ground level pollution.[86] This correlation between $EPFR_v$ and SO_2 is not as strong as $EPFR_v$ with CO or NO, and oil heating is not known to generate EPFRs, so this apparent correlation may stem from meteorological conditions and the formation of a shallow boundary layer. In winter in Xi'an, $EPFR_v$ was found to positively correlate with SO_2 (R^2 > 0.55), suggesting coal combustion as a major source of EPFRs.[11] We observe weak correlation of $EPFR_m$ with SO_2 (Figure S6d), which is consistent with the study in Shihezi, China which also observed very weak correlation.[12]

Generally, O_3 is formed as a result of photochemical processes of NO_x and VOC, but these processes are slow during high-latitude winter, so most regional O_3 should be transported from other regions during winter.[39] In Fairbanks we observe a low mixing ratio of O_3, with an average of 10 ± 7 ppb over the course of the campaign, significantly reduced from the regional background of 30−40 ppb. In this study, we found O_3 to be strongly anticorrelated with $EPFR_v$ with R^2 = 0.65, as shown in Figure 3f. The anticorrelation of EPFR and O_3 is likely to be a result of high abundance of NO_x which titrates O_3 through the reaction NO + O_3 → O_2 + NO_2, as evident from anticorrelation of O_3 in the inversion layer (Figure S9). Since $EPFR_v$ trends with NO_x, this leads to an anticorrelation of EPFRs with O_3. This anticorrelation of $EPFR_v$ with O_3 observed in Fairbanks is similar to our previous study near a highway sampling site, which was also affected by NO titration.[62] In contrast, a study in Xi'an[11] observed a positive correlation of $EPFR_v$ with ozone in the summer, and an annual a positive correlation between $EPFR_m$ and O_3 was observed in Shihezi.[12] A weak correlation between $EPFR_m$ and O_3 is observed (Figure S6e), which indicates that EPFRs are not efficiently quenched by heterogeneous reactions with O_3.

In an attempt to observe correlations without the influence of incomplete combustion, $EPFR_v$ values normalized by EC were compared to the gaseous pollutants (Figure S8). In addition, to minimize the influence of $PM_{2.5}$, we investigated correlations of $EPFR_m$ with $PM_{2.5}$ (Figure S5a) and also plotted the residuals of the correlation between EPFR and $PM_{2.5}$ against the residuals of the gaseous pollutants' correlation with $PM_{2.5}$ (Figure S8). We did not observe significant correlations for these analyses, confirming the strong influence of incomplete combustion and pollutant accumulation in the inversion layer on the observed correlations in Figure 3 (see also Figure S10).

3.4. Correlation of Metals with EPFR Concentration. Figures 4a−f and S11a−f show the correlations of $EPFR_v$ with various metals (Al, Cu, Fe, K, Mg, Mn, Mo, Ni, Pb, Sb, Ti, and Zn). Correlations between $EPFR_m$ and metals are shown in Figure S12. Potassium (K) was the most abundant metal measured at the house site, with average concentration of 93 ± 49 ng m^{-3}, or approximately 0.7% of $PM_{2.5}$ mass. We find that K has a moderate correlation with $EPFR_v$ with R^2 = 0.43

https://doi.org/10.1021/acs.est.4c01206
Environ. Sci. Technol. 2024, 58, 14293−14305

(Figure 4d). K is a marker for biomass burning with potassium salts being internally mixed with soot (elemental carbon), organic carbon, and other components.[87−90] The moderate correlation with K, which is much stronger than that found in Xi'an (R^2 = 0.11),[11] supports that EPFRs are emitted by biomass burning in wintertime in Fairbanks. As there were no wildfires and peat fires during the campaign (wildfire season begins in spring and is extremely rare in winter in Fairbanks), K is emitted most likely from residential wood stoves.

Iron was observed to have the highest metal correlation with $EPFR_v$ with $R^2 > 0.7$. Iron, which is mainly emitted from traffic emissions and biomass burning,[91,92] was the second most abundant metal with an ambient concentration of 43 ± 18 ng m^{-3}. Its concentration reached a peak on the same days when $EPFR_v$ reached its maximums during the warm event, implying the significance of traffic emissions especially by nontailpipe emissions as Fe is emitted substantially by brake wear. Iron and copper have been shown to correlate well with EPFRs at highway sites in Southern California.[62] There is a negligible correlation observed with copper (Cu), and weak correlations observed with molybdenum (Mo) and antimony (Sb) (R^2 < 0.2), which are elements associated with brake wear emissions.[93−96] Copper has been previously shown to stabilize EPFR, but the half-life for copper EPFR stabilization is much shorter than that for iron.[9] While zinc and nickel oxides are very effective to prolong EPFR lifetime,[9] we observe a moderate positive correlation of $EPFR_v$ with Ni and no significant correlation with Zn (Figure S11).

Mineral dust is a major source of iron, aluminum, magnesium, and manganese as well as titanium. Dust was also observed to be a main source of EPFR in Xi'an, China.[11,97] Dust emissions should be low in Fairbanks in the winter due to snow covering up much of the land and soil, and negligible and weak correlations are observed between $EPFR_v$ and Al or Mg emissions in Fairbanks, respectively (R^2 < 0.16). Due to the extremely low temperatures in Fairbanks, rocks or gravel are added to the road for traction in the winter, resulting in road dust that is mostly a combination of crustal minerals. Suspended road salt aerosol was detected by the ATOFMS especially right before the cold event, as neighborhood residents were observed applying salt to entryways and walkways even though the city of Fairbanks does not apply salt to the roads.

Figure 4e,f, show Mn and Ti have moderate and strong correlations with $EPFR_v$, respectively (R^2 > 0.4). These correlations suggest an influence of road dust on EPFRs in Fairbanks. Iron and titanium oxides are known to stabilize EPFRs.[8,9,24,25] Ti is also a major component in brake wear particles.[98] Thus, tight correlations of $EPFR_v$ with Fe and Ti suggests that nontailpipe emissions may play a role in stabilization of EPFR, if they are internally mixed. Since the $PM_{2.5}$ sampler was located in a residential area, the results may vary if compared to a downtown location in Fairbanks where there is more vehicle traffic. As we observe higher $EPFR_v$ during the warm event with greater vehicle emissions and a correlation with titanium throughout the campaign, this supports the importance of vehicular emissions, and the related road dust, to EPFR emissions.

To further examine the existence of iron and PAHs within the same particles, we examined online single-particle mass spectrometry data were examined. Iron was observed in ∼1% of the individual submicron particles (particle diameter of 0.1−1.0 μm), by number, measured by the ATOFMS. Of the identified iron-containing particles, the majority (48%, by number) were identified as residential heating (primarily wood burning) particles with a prominent potassium peak [m/z 39 (K^+)], organic carbon [e.g., m/z 27 ($C_2H_3^+$) and 50 ($C_4H_2^+$)], elemental carbon ($C_n^{\pm}$), and sulfate m/z −97 (HSO_4^-) (Figure 5). PAHs {e.g., naphthalene [m/z 128 ($C_{10}H_8^+$)],

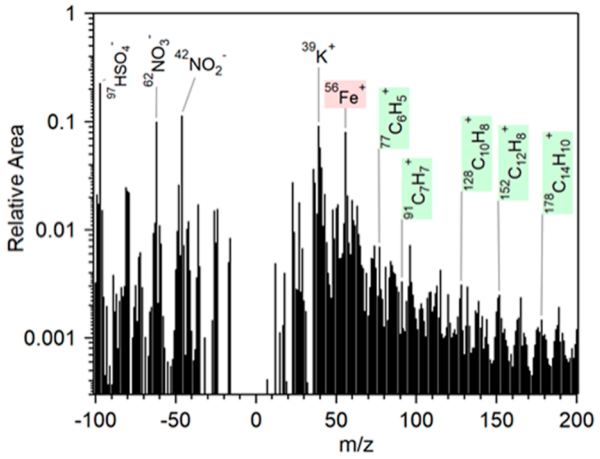

Figure 5. Average dual-polarity mass spectrum [relative ion peak area (arbitrary units) vs mass/charge, m/z], showing negative (left) and positive (right) ions produced within the ATOFMS in the measurement of individual aerosol particles. This mass spectrum is the result of averaging 3109 single-particle mass spectra for only the individual particles that were measured to contain both iron (m/z 56, Fe^+, highlighted in red) and PAHs (prominent PAH molecular ions and fragment ions shaded in green). Additional prominent ions include potassium (m/z 39, K^+) indicative of biomass burning, nitrate (m/z −46, NO_2^-, and −62, NO_3^-), and sulfate (m/z −97, HSO_4^-). Additional unlabeled peaks include elemental carbon clusters ($C_n^{\pm}$, e.g., m/z −36, C_3^+), organic carbon (e.g., m/z 37, C_3H^+), and ammonium (m/z 18, NH_4^+).

acenaphthylene [m/z 152 ($C_{12}H_8^+$)], pyrene and fluoranthene [m/z 202 ($C_{16}H_{10}^+$)] were observed within 60%, by number, of the iron-containing residential heating particles. Higher molecular weight aromatics, including benzofluoranthene/benzopyrene (m/z 252) and benzoperylene/indenopyrene (m/z 276)} were also measured. Previous research has similarly observed that wood/biomass combustion can be a dominant source of Fe-containing aerosol particles.[53,99] Together these results support the coemission and internal mixing of Fe and PAHs from biomass burning. Gasoline and diesel combustion particles accounted for 28% of the iron-containing particles, by number, measured by the ATOFMS. Of the Fe-containing particles from vehicle emissions, 50%, by number, were identified as containing at least one PAH marker ion, supporting vehicle emissions as an additional source of EPFR in Fairbanks. Therefore, the majority of submicrometer particles containing both iron and PAHs are predominantly from residential heating and vehicle emissions. As PAHs are precursors of EPFRs and they can be considered as a proxy for EPFRs, these observations support the conclusion that residential wood burning and vehicle emissions are major sources of EPFR.

4. IMPLICATIONS

We calculated that breathing in Fairbanks winter outdoor air containing EPFRs would be equivalent to smoking on average 0.4−1.0 cigarettes per day, with the minimum being 0.1 and

https://doi.org/10.1021/acs.est.4c01206
Environ. Sci. Technol. 2024, 58, 14293−14305

the maximum being 3.2 cigarettes per day (Table 1). Note that this calculation is based upon outdoor air, while most residents spend much of their time indoors, especially when temperatures outdoors are often far below freezing. The recent study by Yang et al.[100] found that indoor $PM_{2.5}$ mass concentration was found to be significantly lower than outdoors in Fairbanks during the ALPACA campaign, while indoor $PM_{2.5}$ concentrations can be greatly enhanced by indoor activities including pellet burning and cooking.[100] From an exposure perspective, EPFR cigarette equivalence should be studied for outdoor air, infiltrated air, and air influenced by indoor sourced pollution. Gehling and Dellinger[15] concluded that 0.4−0.9 cigarettes per day would represent nonextreme air quality (35−60 μg $PM_{2.5}$/m^3 average over 24 h). Therefore, Fairbanks primarily has nonextreme air quality, but may be a concern for public health after prolonged temperature inversion in which we observe higher concentration of EPFRs (see Section 3.2). As shown in Table 1, this value in Fairbanks is comparable to that in Irvine, CA,[62] but lower than those in highly polluted Chinese cities including Shihezi,[12] Xi'an,[11] and Beijing.[5]

EPFRs with a semiquinone type structure are known to be redox active, which means that they can induce the formation of ROS upon inhalation and respiratory deposition to lung lining fluid, causing oxidative stress and adverse health effects.[76,101,102] EPFRs can reduce molecular oxygen to superoxide radicals,[103] which can then be transformed to •OH that can induce oxidative damage to biomolecules including proteins and lipids if it overwhelms antioxidants.[102] As shown in Figure 6, we observe that OP_v^{OH} correlates

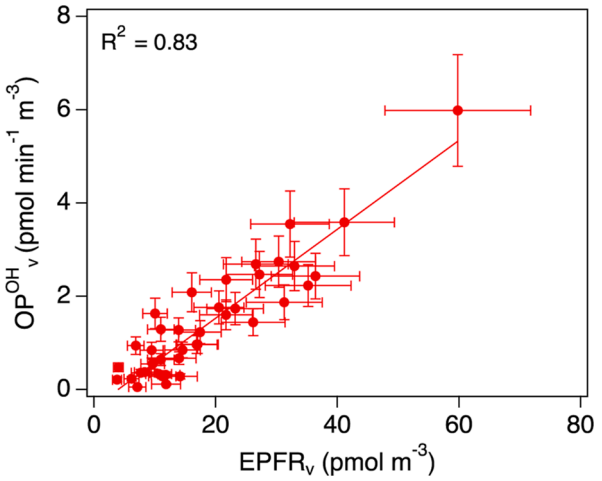

Figure 6. Correlation between OP^{OH}_v (pmol min^{-1} m^{-3}) and $EPFR_v$ (pmol m^{-3}). The correlation of OP^{OH} with $EPFR_v$ has a p-value < 0.01.

strongly with $EPFR_v$ with R^2 = 0.83. This tight correlation suggests that EPFRs are strongly related to •OH production in surrogate lung fluid. It also indicates an important role of lung antioxidants as a previous study observed a moderate correlation of EPFRs with OH formation in water.[62] Our results imply that exposure to EPFRs and inhalation and respiratory deposition of PM may cause oxidative stress and adverse health effects. A very recent study has observed a positive correlation between cytotoxicity and EPFR concentration.[104] Another recent study by Yang et al. (2024) showed that PM oxidative potential in Fairbanks is comparable to that in Atlanta and Los Angeles.[105] As the relationship between PM oxidative potential and ROS formation is complex and remain unelucidated,[106] in our follow-up study we plan to investigate ROS and oxidative potential by PM collected in the atmosphere and in a house in Fairbanks during the ALPACA campaign.

■ ASSOCIATED CONTENT

Supporting Information

The Supporting Information is available free of charge at https://pubs.acs.org/doi/10.1021/acs.est.4c01206.

Includes sample EPFR spectra and calibration curve with TEMPOL. Correlations of relative humidity and temperature with EPFR shown. EPFR signal after 6 months plotted. Includes gas, metal, and particle data plotted against $EPFR_m$. Gas correlations shown with $PM_{2.5}$, $EPFR_m$, $EPFR_{EC}$, as well as with residuals between EPFR and $PM_{2.5}$. O_3 correlation with inversion time shown. $EPFR_m$ correlations with metals shown. Includes LOD of metals (PDF)

■ AUTHOR INFORMATION

Corresponding Author

Manabu Shiraiwa − *Department of Chemistry, University of California, Irvine, Irvine, California 92697, United States;* orcid.org/0000-0003-2532-5373; Email: m.shiraiwa@uci.edu

Authors

Kasey C. Edwards − *Department of Chemistry, University of California, Irvine, Irvine, California 92697, United States*

Sukriti Kapur − *Department of Chemistry, University of California, Irvine, Irvine, California 92697, United States;* orcid.org/0000-0001-6645-7300

Ting Fang − *Department of Chemistry, University of California, Irvine, Irvine, California 92697, United States; Sustainable Energy and Environment Thrust, The Hong Kong University of Science and Technology (Guangzhou), Guangzhou, Guangdong 511400, China;* orcid.org/0000-0002-4845-2749

Meeta Cesler-Maloney − *Department of Chemistry and Biochemistry, University of Alaska, Fairbanks, Fairbanks, Alaska 99775, United States*

Yuhan Yang − *School of Earth and Atmospheric Sciences, Georgia Institute of Technology, Atlanta, Georgia 30332, United States;* orcid.org/0000-0003-0343-3429

Andrew L. Holen − *Department of Chemistry, University of Michigan, Ann Arbor, Michigan 48109, United States;* orcid.org/0009-0006-7654-2019

Judy Wu − *Department of Chemistry, University of Michigan, Ann Arbor, Michigan 48109, United States;* orcid.org/0000-0003-3541-4492

Ellis S. Robinson − *Department of Environmental Health and Engineering, Johns Hopkins University, Baltimore, Maryland 21212, United States;* orcid.org/0000-0003-1695-6392

Peter F. DeCarlo − *Department of Environmental Health and Engineering, Johns Hopkins University, Baltimore, Maryland 21212, United States;* orcid.org/0000-0001-6385-7149

Kerri A. Pratt − *Department of Chemistry, University of Michigan, Ann Arbor, Michigan 48109, United States; Department of Earth and Environmental Sciences, University of Michigan, Ann Arbor, Michigan 48109, United States;* orcid.org/0000-0003-4707-2290

https://doi.org/10.1021/acs.est.4c01206
Environ. Sci. Technol. 2024, 58, 14293−14305

Rodney J. Weber − *School of Earth and Atmospheric Sciences, Georgia Institute of Technology, Atlanta, Georgia 30332, United States;* orcid.org/0000-0003-0765-8035

William R. Simpson − *Department of Chemistry and Biochemistry, University of Alaska, Fairbanks, Fairbanks, Alaska 99775, United States;* orcid.org/0000-0002-8596-7290

Complete contact information is available at: https://pubs.acs.org/10.1021/acs.est.4c01206

Notes

The authors declare no competing financial interest.

■ ACKNOWLEDGMENTS

The authors declare that they have no conflict of interest. We thank the entire ALPACA science team of researchers for designing the experiment, acquiring funding, making measurements, and ongoing analysis of the results. The ALPACA project was initiated as a part of PACES under IGAC and with support of IASC. We thank University of Alaska Fairbanks and the Geophysical Institute for logistical support, and we thank Fairbanks for welcoming and engaging with this research. K.C.E., S.K., T.F., and M.S. acknowledge funding from the U.S. National Science Foundation (AGS-1654104, CHE-2203419). M.C.-M. and W.R.S. acknowledge support from NSF grants NNA-1927750 and AGS-2109134. Y.Y. and R.J.W. were supported by the National Science Foundation's (NSF) Atmospheric Geoscience Program grant no. AGS-2029730 and the NSF Navigating the New Arctic Program grant no. NNA-1927778. A.L.H., J.W., and K.A.P. acknowledge support from NSF grant RISE-1927831. E.S.R. and P.F.D. acknowledge support from the U.S. National Science Foundation's Navigating the New Arctic Program under grants NNA-90086753 and NNA-1927750.

■ REFERENCES

(1) Gehling, W.; Khachatryan, L.; Dellinger, B. Hydroxyl Radical Generation from Environmentally Persistent Free Radicals (EPFRs) in PM2.5. *Environ. Sci. Technol.* **2014**, *48* (8), 4266−4272.

(2) Pan, B.; Li, H.; Lang, D.; Xing, B. Environmentally persistent free radicals: Occurrence, formation mechanisms and implications. *Environ. Pollut.* **2019**, *248*, 320−331.

(3) Xu, M.; Wu, T.; Tang, Y.-T.; Chen, T.; Khachatryan, L.; Iyer, P. R.; Guo, D.; Chen, A.; Lyu, M.; Li, J.; Liu, J.; Li, D.; Zuo, Y.; Zhang, S.; Wang, Y.; Meng, Y.; Qi, F. Environmentally persistent free radicals in PM2.5: a review. *Waste Dispos. Sustain. Energy* **2019**, *1* (3), 177−197.

(4) Shiraiwa, M.; Ueda, K.; Pozzer, A.; Lammel, G.; Kampf, C. J.; Fushimi, A.; Enami, S.; Arangio, A. M.; Fröhlich-Nowoisky, J.; Fujitani, Y.; Furuyama, A.; Lakey, P. S. J.; Lelieveld, J.; Lucas, K.; Morino, Y.; Pöschl, U.; Takahama, S.; Takami, A.; Tong, H. J.; Weber, B.; Yoshino, A.; Sato, K. Aerosol Health Effects from Molecular to Global Scales. *Environ. Sci. Technol.* **2017**, *51* (23), 13545−13567.

(5) Yang, L.; Liu, G.; Zheng, M.; Jin, R.; Zhu, Q.; Zhao, Y.; Wu, X.; Xu, Y. Highly Elevated Levels and Particle-Size Distributions of Environmentally Persistent Free Radicals in Haze-Associated Atmosphere. *Environ. Sci. Technol.* **2017**, *51* (14), 7936−7944.

(6) Odinga, E. S.; Waigi, M. G.; Gudda, F. O.; Wang, J.; Yang, B.; Hu, X.; Li, S.; Gao, Y. Occurrence, formation, environmental fate and risks of environmentally persistent free radicals in biochars. *Environ. Int.* **2020**, *134*, 105172.

(7) Zhao, J.; Shen, G.; Shi, L.; Li, H.; Lang, D.; Zhang, L.; Pan, B.; Tao, S. Real-World Emission Characteristics of Environmentally Persistent Free Radicals in PM2.5 from Residential Solid Fuel Combustion. *Environ. Sci. Technol.* **2022**, *56* (7), 3997−4004.

(8) Vejerano, E.; Lomnicki, S.; Dellinger, B. Lifetime of combustion-generated environmentally persistent free radicals on Zn(II)O and other transition metal oxides. *J. Environ. Monit* **2012**, *14* (10), 2803−2806.

(9) Vejerano, E.; Lomnicki, S.; Dellinger, B. Formation and Stabilization of Combustion-Generated Environmentally Persistent Free Radicals on an Fe(III)2O3/Silica Surface. *Environ. Sci. Technol.* **2011**, *45* (2), 589−594.

(10) Chen, Q.; Sun, H.; Wang, J.; Shan, M.; Yang, X.; Deng, M.; Wang, Y.; Zhang, L. Long-life type — The dominant fraction of EPFRs in combustion sources and ambient fine particles in Xi'an. *Atmos. Environ.* **2019**, *219*, 117059.

(11) Chen, Q.; Sun, H.; Mu, Z.; Wang, Y.; Li, Y.; Zhang, L.; Wang, M.; Zhang, Z. Characteristics of environmentally persistent free radicals in PM2.5: Concentrations, species and sources in Xi'an, Northwestern China. *Environ. Pollut.* **2019**, *247*, 18−26.

(12) He, F.; Lu, J.; Li, Z.; Li, M.; Liu, Z.; Tong, Y. Characteristics of Environmentally Persistent Free Radicals in PM2.5 and the Influence of Air Pollutants in Shihezi, Northwestern China. *Toxics* **2022**, *10* (7), 341.

(13) Xu, Y.; Qin, L.; Liu, G.; Zheng, M.; Li, D.; Yang, L. Assessment of personal exposure to environmentally persistent free radicals in airborne particulate matter. *J. Hazard. Mater.* **2021**, *409*, 125014.

(14) Johnson, E. P. Carbon footprints of heating oil and LPG heating systems. *Environ. Impact Assess. Rev.* **2012**, *35*, 11−22.

(15) Gehling, W.; Dellinger, B. Environmentally Persistent Free Radicals and Their Lifetimes in PM2.5. *Environ. Sci. Technol.* **2013**, *47* (15), 8172−8178.

(16) Chen, Q.; Sun, H.; Wang, M.; Mu, Z.; Wang, Y.; Li, Y.; Wang, Y.; Zhang, L.; Zhang, Z. Dominant Fraction of EPFRs from Nonsolvent-Extractable Organic Matter in Fine Particulates over Xi'an, China. *Environ. Sci. Technol.* **2018**, *52* (17), 9646−9655.

(17) Ahmad, M.; Chen, J.; Yu, Q.; Tariq Khan, M.; Weqas Ali, S.; Nawab, A.; Phairuang, W.; Panyametheekul, S. Characteristics and Risk Assessment of Environmentally Persistent Free Radicals (EPFRs) of PM2.5 in Lahore, Pakistan. *Int. J. Environ. Res. Publ. Health* **2023**, *20* (3), 2384.

(18) Arangio, A. M.; Tong, H.; Socorro, J.; Pöschl, U.; Shiraiwa, M. Quantification of environmentally persistent free radicals and reactive oxygen species in atmospheric aerosol particles. *Atmos. Chem. Phys.* **2016**, *16* (20), 13105−13119.

(19) Valavanidis, A.; Fiotakis, K.; Bakeas, E.; Vlahogianni, T. Electron paramagnetic resonance study of the generation of reactive oxygen species catalysed by transition metals and quinoid redox cycling by inhalable ambient particulate matter. *Redox Rep.* **2005**, *10* (1), 37−51.

(20) Balakrishna, S.; Lomnicki, S.; McAvey, K. M.; Cole, R. B.; Dellinger, B.; Cormier, S. A. Environmentally persistent free radicals amplify ultrafine particle mediated cellular oxidative stress and cytotoxicity. *Part. Fibre Toxicol.* **2009**, *6* (1), 11.

(21) Balakrishna, S.; Saravia, J.; Thevenot, P.; Ahlert, T.; Lominiki, S.; Dellinger, B.; Cormier, S. A. Environmentally persistent free radicals induce airway hyperresponsiveness in neonatal rat lungs. *Part. Fibre Toxicol.* **2011**, *8* (1), 11.

(22) Kelley, M. A.; Hebert, V. Y.; Thibeaux, T. M.; Orchard, M. A.; Hasan, F.; Cormier, S. A.; Thevenot, P. T.; Lomnicki, S. M.; Varner, K. J.; Dellinger, B.; Latimer, B. M.; et al. Model combustion-generated particulate matter containing persistent free radicals redox cycle to produce reactive oxygen species. *Chem. Res. Toxicol.* **2013**, *26* (12), 1862−1871.

(23) Feld-Cook, E. E.; Bovenkamp-Langlois, L.; Lomnicki, S. M. Effect of Particulate Matter Mineral Composition on Environmentally Persistent Free Radical (EPFR) Formation. *Environ. Sci. Technol.* **2017**, *51* (18), 10396−10402.

(24) Dellinger, B.; Lomnicki, S.; Khachatryan, L.; Maskos, Z.; Hall, R. W.; Adounkpe, J.; McFerrin, C.; Truong, H. Formation and stabilization of persistent free radicals. *Proc. Combust. Inst.* **2007**, *31* (1), 521−528.

(25) Yang, L.; Liu, G.; Zheng, M.; Jin, R.; Zhao, Y.; Wu, X.; Xu, Y. Pivotal Roles of Metal Oxides in the Formation of Environmentally Persistent Free Radicals. *Environ. Sci. Technol.* **2017**, *51* (21), 12329−12336.
(26) Liu, S.; Liu, G.; Yang, L.; Li, D.; Zheng, M. Critical influences of metal compounds on the formation and stabilization of environmentally persistent free radicals. *Chem. Eng. J.* **2022**, *427*, 131666.
(27) Chen, Q.; Sun, H.; Wang, M.; Wang, Y.; Zhang, L.; Han, Y. Environmentally Persistent Free Radical (EPFR) Formation by Visible-Light Illumination of the Organic Matter in Atmospheric Particles. *Environ. Sci. Technol.* **2019**, *53* (17), 10053−10061.
(28) Zhu, J.; Sheng, M.; Shang, J.; Kuang, Y.; Shi, X.; Qiu, X. Photocatalytic Role of Atmospheric Soot Particles under Visible-Light Irradiation: Reactive Oxygen Species Generation, Self-Oxidation Process, and Induced Higher Oxidative Potential and Cytotoxicity. *Environ. Sci. Technol.* **2022**, *56* (12), 7668−7678.
(29) Sarmiento, D. J.; Majestic, B. J. Formation of Environmentally Persistent Free Radicals from the Irradiation of Polycyclic Aromatic Hydrocarbons. *J. Phys. Chem. A* **2023**, *127* (25), 5390−5401.
(30) Tran, H. N. Q.; Mölders, N. Investigations on meteorological conditions for elevated PM2.5 in Fairbanks, Alaska. *Atmos. Res.* **2011**, *99* (1), 39−49.
(31) Malingowski, J.; Atkinson, D.; Fochesatto, J.; Cherry, J.; Stevens, E. An observational study of radiation temperature inversions in Fairbanks, Alaska. *Polar Sci.* **2014**, *8* (1), 24−39.
(32) Coutts, H. J. *Study of Winter Air Pollutants at Fairbanks, Alaska. Final Report, 1976−1979*; Corvallis Environmental Research Lab., College, AK (USA). Arctic Environmental Research Station, 1979. https://www.osti.gov/biblio/5196630 (accessed 2022/06/21/15:17:40).
(33) Ye, L.; Wang, Y. Long-Term Air Quality Study in Fairbanks, Alaska: Air Pollutant Temporal Variations, Correlations, and $PM_{2.5}$ Source Apportionment. *Atmosphere* **2020**, *11* (11), 1203.
(34) Cesler-Maloney, M.; Simpson, W. R.; Miles, T.; Mao, J.; Law, K. S.; Roberts, T. J. Differences in Ozone and Particulate Matter Between Ground Level and 20 m Aloft are Frequent During Wintertime Surface-Based Temperature Inversions in Fairbanks, Alaska. *J. Geophys. Res. Atmos.* **2022**, *127* (10), No. e2021JD036215.
(35) Schmale, J.; Arnold, S. R.; Law, K. S.; Thorp, T.; Anenberg, S.; Simpson, W. R.; Mao, J.; Pratt, K. A. Local Arctic Air Pollution: A Neglected but Serious Problem. *Earth's Future* **2018**, *6* (10), 1385−1412.
(36) Ward, T.; Trost, B.; Conner, J.; Flanagan, J.; Jayanty, R. K. M. Source Apportionment of PM2.5 in a Subarctic Airshed - Fairbanks, Alaska. *Aerosol Air Qual. Res.* **2012**, *12* (4), 536−543.
(37) Wang, Y.; Hopke, P. K. Is Alaska Truly the Great Escape from Air Pollution? - Long Term Source Apportionment of Fine Particulate Matter in Fairbanks, Alaska. *Aerosol Air Qual. Res.* **2014**, *14* (7), 1875−1882.
(38) Robinson, E. S.; Cesler-Maloney, M.; Tan, X.; Mao, J.; Simpson, W.; DeCarlo, P. F. Wintertime spatial patterns of particulate matter in Fairbanks, AK during ALPACA 2022. *Environ. Sci.: Atmos.* **2023**, *3* (3), 568−580.
(39) Simpson, W. R.; Mao, J.; Fochesatto, G. J.; Law, K. S.; DeCarlo, P. F.; Schmale, J.; Pratt, K. A.; Arnold, S. R.; Stutz, J.; Dibb, J. E.; Creamean, J. M.; Weber, R. J.; Williams, B. J.; Alexander, B.; Hu, L.; Yokelson, R. J.; Shiraiwa, M.; Decesari, S.; Anastasio, C.; D'Anna, B.; Gilliam, R. C.; Nenes, A.; St. Clair, J. M.; Trost, B.; Flynn, J. H.; Savarino, J.; Conner, L. D.; Kettle, N.; Heeringa, K. M.; Albertin, S.; Baccarini, A.; Barret, B.; Battaglia, M. A.; Bekki, S.; Brado, T. J.; Brett, N.; Brus, D.; Campbell, J. R.; Cesler-Maloney, M.; Cooperdock, S.; Cysneiros de Carvalho, K.; Delbarre, H.; DeMott, P. J.; Dennehy, C. J. S.; Dieudonné, E.; Dingilian, K. K.; Donateo, A.; Doulgeris, K. M.; Edwards, K. C.; Fahey, K.; Fang, T.; Guo, F.; Heinlein, L. M. D.; Holen, A. L.; Huff, D.; Ijaz, A.; Johnson, S.; Kapur, S.; Ketcherside, D. T.; Levin, E.; Lill, E.; Moon, A. R.; Onishi, T.; Pappaccogli, G.; Perkins, R.; Pohorsky, R.; Raut, J.-C.; Ravetta, F.; Roberts, T.; Robinson, E. S.; Scoto, F.; Selimovic, V.; Sunday, M. O.; Temime-Roussel, B.; Tian, X.; Wu, J.; Yang, Y. Overview of the Alaskan Layered Pollution and Chemical Analysis (ALPACA) Field Experiment. *ACS ES&T Air* **2024**, *1* (3), 200−222.
(40) Schober, P.; Boer, C.; Schwarte, L. A. Correlation Coefficients: Appropriate Use and Interpretation. *Anesth. Analg.* **2018**, *126* (5), 1763−1768.
(41) Birch, M. E.; Cary, R. A. Elemental Carbon-Based Method for Monitoring Occupational Exposures to Particulate Diesel Exhaust. *Aerosol Sci. Technol.* **1996**, *25* (3), 221−241.
(42) Ulbrich, I. M.; Canagaratna, M. R.; Zhang, Q.; Worsnop, D. R.; Jimenez, J. L. Interpretation of organic components from Positive Matrix Factorization of aerosol mass spectrometric data. *Atmos. Chem. Phys.* **2009**, *9* (9), 2891−2918.
(43) Robinson, E. S.; Battaglia Jr, M.; Campbell, J. R.; Cesler-Maloney, M.; Simpson, W.; Mao, J.; Weber, R. J.; DeCarlo, P. Multi-year, high-time resolution aerosol chemical composition and mass measurements from Fairbanks, Alaska. *Environ. Sci.: Atmos.* **2024**, *4*, 685−698.
(44) Dzepina, K.; Arey, J.; Marr, L. C.; Worsnop, D. R.; Salcedo, D.; Zhang, Q.; Onasch, T. B.; Molina, L. T.; Molina, M. J.; Jimenez, J. L. Detection of particle-phase polycyclic aromatic hydrocarbons in Mexico City using an aerosol mass spectrometer. *Int. J. Mass Spectrom.* **2007**, *263* (2−3), 152−170.
(45) Poulain, L.; Iinuma, Y.; Müller, K.; Birmili, W.; Weinhold, K.; Brüggemann, E.; Gnauk, T.; Hausmann, A.; Löschau, G.; Wiedensohler, A.; Herrmann, H. Diurnal variations of ambient particulate wood burning emissions and their contribution to the concentration of Polycyclic Aromatic Hydrocarbons (PAHs) in Seiffen, Germany. *Atmos. Chem. Phys.* **2011**, *11* (24), 12697−12713.
(46) Yang, Y.; Gao, D.; Weber, R. J. A method for liquid spectrophotometric measurement of total and water-soluble iron and copper in ambient aerosols. *Atmos. Meas. Tech.* **2021**, *14* (6), 4707−4719.
(47) Campisano, R.; Hall, K.; Griggs, J.; Willison, S.; Reimer, S.; Mash, H.; Magnuson, M.; Boczek, L.; Rhodes, E. *Selected Analytical Methods for Environmental Remediation and Recovery (SAM) 2017*; U.S Environmental Protection Agency: Washington, DC, EPA/600/R-17/356, 2017.
(48) Pratt, K. A.; Mayer, J. E.; Holecek, J. C.; Moffet, R. C.; Sanchez, R. O.; Rebotier, T. P.; Furutani, H.; Gonin, M.; Fuhrer, K.; Su, Y.; Guazzotti, S.; Prather, K. A. Development and characterization of an aircraft aerosol time-of-flight mass spectrometer. *Anal. Chem.* **2009**, *81* (5), 1792−1800.
(49) Gunsch, M. J.; Kirpes, R. M.; Kolesar, K. R.; Barrett, T. E.; China, S.; Sheesley, R. J.; Laskin, A.; Wiedensohler, A.; Tuch, T.; Pratt, K. A. Contributions of transported Prudhoe Bay oil field emissions to the aerosol population in Utqiaġvik, Alaska. *Atmos. Chem. Phys.* **2017**, *17* (17), 10879−10892.
(50) Sultana, C. M.; Cornwell, G. C.; Rodriguez, P.; Prather, K. A. FATES: a flexible analysis toolkit for the exploration of single-particle mass spectrometer data. *Atmos. Meas. Tech.* **2017**, *10* (4), 1323−1334.
(51) Song, X.-H.; Hopke, P. K.; Fergenson, D. P.; Prather, K. A. Classification of Single Particles Analyzed by ATOFMS Using an Artificial Neural Network, ART-2A. *Anal. Chem.* **1999**, *71* (4), 860−865.
(52) Dall'Osto, M.; Beddows, D. C. S.; Harrison, R. M.; Onat, B. Fine Iron Aerosols Are Internally Mixed with Nitrate in the Urban European Atmosphere. *Environ. Sci. Technol.* **2016**, *50* (8), 4212−4220.
(53) Furutani, H.; Jung, J.; Miura, K.; Takami, A.; Kato, S.; Kajii, Y.; Uematsu, M. Single-particle chemical characterization and source apportionment of iron-containing atmospheric aerosols in Asian outflow. *J. Geophys. Res. Atmos.* **2011**, *116* (D18), D18204.
(54) Silva, P. J.; Prather, K. A. Interpretation of mass spectra from organic compounds in aerosol time-of-flight mass spectrometry. *Anal. Chem.* **2000**, *72* (15), 3553−3562.
(55) Dall'Osto, M.; Harrison, R. M. Urban organic aerosols measured by single particle mass spectrometry in the megacity of London. *Atmos. Chem. Phys.* **2012**, *12* (9), 4127−4142.

(56) Passig, J.; Schade, J.; Irsig, R.; Kröger-Badge, T.; Czech, H.; Adam, T.; Fallgren, H.; Moldanova, J.; Sklorz, M.; Streibel, T.; Zimmermann, R. Single-particle characterization of polycyclic aromatic hydrocarbons in background air in northern Europe. *Atmos. Chem. Phys.* **2022**, *22* (2), 1495−1514.
(57) Charrier, J. G.; McFall, A. S.; Vu, K. K. T.; Baroi, J.; Olea, C.; Hasson, A.; Anastasio, C. A bias in the "mass-normalized" DTT response - an effect of non-linear concentration-response curves for copper and manganese. *Atmos. Environ.* **2016**, *144*, 325−334.
(58) Gao, D.; Fang, T.; Verma, V.; Zeng, L.; Weber, R. J. A method for measuring total aerosol oxidative potential (OP) with the dithiothreitol (DTT) assay and comparisons between an urban and roadside site of water-soluble and total OP. *Atmos. Meas. Tech.* **2017**, *10* (8), 2821−2835.
(59) Yu, H.; Puthussery, J. V.; Wang, Y.; Verma, V. Spatiotemporal variability in the oxidative potential of ambient fine particulate matter in the Midwestern United States. *Atmos. Chem. Phys.* **2021**, *21* (21), 16363−16386.
(60) Guo, C.; Richmond-Bryant, J. A critical review of environmentally persistent free radical (EPFR) solvent extraction methodology and retrieval efficiency. *Chemosphere* **2021**, *284*, 131353.
(61) Wang, Y.; Yao, K.; Fu, X. e.; Zhai, X.; Jin, L.; Guo, H. Size-resolved exposure risk and subsequent role of environmentally persistent free radicals (EPFRs) from atmospheric particles. *Atmos. Environ.* **2022**, *276*, 119059.
(62) Hwang, B.; Fang, T.; Pham, R.; Wei, J.; Gronstal, S.; Lopez, B.; Frederickson, C.; Galeazzo, T.; Wang, X.; Jung, H.; Shiraiwa, M. Environmentally Persistent Free Radicals, Reactive Oxygen Species Generation, and Oxidative Potential of Highway PM2.5. *ACS Earth Space Chem.* **2021**, *5* (8), 1865−1875.
(63) Fang, T. H.; Hwang, B. C.; Kapur, S. S.; Hopstock, K.; Wei, J.; Nguyen, V. A.; Nizkorodov, S.; Shiraiwa, M. Wildfire particulate matter as a source of environmentally persistent free radicals and reactive oxygen species. *Environ. Sci.: Atmos.* **2023**, *3* (3), 581−594.
(64) Filippi, A.; Sheu, R.; Berkemeier, T.; Pöschl, U.; Tong, H. R.; Gentner, D. Environmentally persistent free radicals in indoor particulate matter, dust, and on surfaces. *Environ. Sci.: Atmos.* **2022**, *2* (2), 128−136.
(65) Chen, Q.; Sun, H.; Song, W.; Cao, F.; Tian, C.; Zhang, Y.-L. Size-resolved exposure risk of persistent free radicals (PFRs) in atmospheric aerosols and their potential sources. *Atmos. Chem. Phys.* **2020**, *20* (22), 14407−14417.
(66) Kotchenruther, R. A. Recent changes in winter PM2.5 contributions from wood smoke, motor vehicles, and other sources in the Northwest U.S. *Atmos. Environ.* **2020**, *237*, 117724.
(67) Karanasiou, A.; Minguillón, M. C.; Viana, M.; Alastuey, A.; Putaud, J. P.; Maenhaut, W.; Panteliadis, P.; Močnik, G.; Favez, O.; Kuhlbusch, T. a. J. Thermal-optical analysis for the measurement of elemental carbon (EC) and organic carbon (OC) in ambient air a literature review. *Atmos. Meas. Tech. Discuss.* **2015**, *8* (9), 9649−9712.
(68) Yang, H.-H.; Dhital, N. B.; Wang, L.-C.; Hsieh, Y.-S.; Lee, K.-T.; Hsu, Y.-T.; Huang, S.-C. Chemical Characterization of Fine Particulate Matter in Gasoline and Diesel Vehicle Exhaust. *Aerosol Air Qual. Res.* **2019**, *19* (6), 1439−1449.
(69) Peng, Y.; Cai, J.; Feng, Y.; Jiang, H.; Chen, Y. Emission characteristic of OVOCs, I/SVOCs, OC and EC from wood combustion at different moisture contents. *Atmos. Environ.* **2023**, *298*, 119620.
(70) Noll, J. D.; Bugarski, A. D.; Patts, L. D.; Mischler, S. E.; McWilliams, L. Relationship between Elemental Carbon, Total Carbon, and Diesel Particulate Matter in Several Underground Metal/Non-metal Mines. *Environ. Sci. Technol.* **2007**, *41* (3), 710−716.
(71) Schauer, J. J. Evaluation of elemental carbon as a marker for diesel particulate matter. *J. Expo. Sci. Environ. Epidemiol.* **2003**, *13* (6), 443−453.
(72) Zeng, T.; Wang, Y. Nationwide summer peaks of OC/EC ratios in the contiguous United States. *Atmos. Environ.* **2011**, *45* (3), 578−586.
(73) Liu, F.; Joo, T.; Ditto, J. C.; Saavedra, M. G.; Takeuchi, M.; Boris, A. J.; Yang, Y.; Weber, R. J.; Dillner, A. M.; Gentner, D. R.; Ng, N. L. Oxidized and Unsaturated: Key Organic Aerosol Traits Associated with Cellular Reactive Oxygen Species Production in the Southeastern United States. *Environ. Sci. Technol.* **2023**, *57* (38), 14150−14161.
(74) Kostenidou, E.; Florou, K.; Kaltsonoudis, C.; Tsiflikiotou, M.; Vratolis, S.; Eleftheriadis, K.; Pandis, S. N. Sources and chemical characterization of organic aerosol during the summer in the eastern Mediterranean. *Atmos. Chem. Phys.* **2015**, *15* (19), 11355−11371.
(75) Kuang, Y.; Huang, S.; Xue, B.; Luo, B.; Song, Q.; Chen, W.; Hu, W.; Li, W.; Zhao, P.; Cai, M.; Peng, Y.; Qi, J.; Li, T.; Wang, S.; Chen, D.; Yue, D.; Yuan, B.; Shao, M. Contrasting effects of secondary organic aerosol formations on organic aerosol hygroscopicity. *Atmos. Chem. Phys.* **2021**, *21* (13), 10375−10391.
(76) Zhao, Z.; Li, H.; Wei, Y.; Fang, G.; Jiang, Q.; Pang, Y.; Huang, W.; Tang, M.; Jing, Y.; Feng, X.; Luo, X.-S.; Berkemeier, T. Airborne environmentally persistent free radicals (EPFRs) in PM2.5 from combustion sources: Abundance, cytotoxicity and potential exposure risks. *Sci. Total Environ.* **2024**, *927*, 172202.
(77) Weilenmann, M.; Favez, J.-Y.; Alvarez, R. Cold-start emissions of modern passenger cars at different low ambient temperatures and their evolution over vehicle legislation categories. *Atmos. Environ.* **2009**, *43* (15), 2419−2429.
(78) Zhu, R.; Wei, Y.; He, L.; Wang, M.; Hu, J.; Li, Z.; Lai, Y.; Su, S. Particulate matter emissions from light-duty gasoline vehicles under different ambient temperatures: Physical properties and chemical compositions. *Sci. Total Environ.* **2024**, *926*, 171791.
(79) Krauss, M.; Wilcke, W.; Martius, C.; Bandeira, A. G.; Garcia, M. V. B.; Amelung, W. Atmospheric versus biological sources of polycyclic aromatic hydrocarbons (PAHs) in a tropical rain forest environment. *Environ. Pollut.* **2005**, *135* (1), 143−154.
(80) Ma, W.-L.; Li, Y.-F.; Qi, H.; Sun, D.-Z.; Liu, L.-Y.; Wang, D.-G. Seasonal variations of sources of polycyclic aromatic hydrocarbons (PAHs) to a northeastern urban city, China. *Chemosphere* **2010**, *79* (4), 441−447.
(81) Howsam, M.; Jones, K. C. Sources of PAHs in the Environment. In *PAHs and Related Compounds: Chemistry*; Neilson, A. H., Ed.; The Handbook of Environmental Chemistry; Springer, 1998; pp 137−174.
(82) Abdel-Shafy, H. I.; Mansour, M. S. M. A review on polycyclic aromatic hydrocarbons: Source, environmental impact, effect on human health and remediation. *Egypt. J. Pet.* **2016**, *25* (1), 107−123.
(83) Ozgen, S.; Cernuschi, S.; Caserini, S. An overview of nitrogen oxides emissions from biomass combustion for domestic heat production. *Renewable and Sustainable Energy Reviews* **2021**, *135*, 110113.
(84) McDonald, B. C.; Dallmann, T. R.; Martin, E. W.; Harley, R. A. Long-term trends in nitrogen oxide emissions from motor vehicles at national, state, and air basin scales. *J. Geophys. Res. Atmos.* **2012**, *117* (D21), D00V18.
(85) Shakya, K. M.; Peltier, R. E. Investigating Missing Sources of Sulfur at Fairbanks, Alaska. *Environ. Sci. Technol.* **2013**, *47* (16), 9332−9338.
(86) Tran, H. N. Q.; Mölders, N. Numerical investigations on the contribution of point source emissions to the PM2.5 concentrations in Fairbanks, Alaska. *Atmos. Pollut. Res.* **2012**, *3* (2), 199−210.
(87) Yu, J.; Yan, C.; Liu, Y.; Li, X.; Zhou, T.; Zheng, M. Potassium: A Tracer for Biomass Burning in Beijing? *Aerosol Air Qual. Res.* **2018**, *18* (9), 2447−2459.
(88) Pio, C. A.; Legrand, M.; Alves, C. A.; Oliveira, T.; Afonso, J.; Caseiro, A.; Puxbaum, H.; Sanchez-Ochoa, A.; Gelencsér, A. Chemical composition of atmospheric aerosols during the 2003 summer intense forest fire period. *Atmos. Environ.* **2008**, *42* (32), 7530−7543.
(89) Achad, M.; Caumo, S.; de Castro Vasconcellos, P.; Bajano, H.; Gómez, D.; Smichowski, P. Chemical markers of biomass burning: Determination of levoglucosan, and potassium in size-classified

atmospheric aerosols collected in Buenos Aires, Argentina by different analytical techniques. *Microchem. J.* **2018**, *139*, 181−187.
(90) Freney, E. J.; Martin, S. T.; Buseck, P. R. Deliquescence and Efflorescence of Potassium Salts Relevant to Biomass-Burning Aerosol Particles. *Aerosol Sci. Technol.* **2009**, *43* (8), 799−807.
(91) Luo, C.; Mahowald, N.; Bond, T.; Chuang, P. Y.; Artaxo, P.; Siefert, R.; Chen, Y.; Schauer, J. Combustion iron distribution and deposition. *Global Biogeochem. Cycles* **2008**, *22* (1), GB1012.
(92) Matsui, H.; Mahowald, N. M.; Moteki, N.; Hamilton, D. S.; Ohata, S.; Yoshida, A.; Koike, M.; Scanza, R. A.; Flanner, M. G. Anthropogenic combustion iron as a complex climate forcer. *Nat. Commun.* **2018**, *9* (1), 1593.
(93) Iijima, A.; Sato, K.; Yano, K.; Kato, M.; Kozawa, K.; Furuta, N. Emission Factor for Antimony in Brake Abrasion Dusts as One of the Major Atmospheric Antimony Sources. *Environ. Sci. Technol.* **2008**, *42* (8), 2937−2942.
(94) Wong, M. Y.; Rathod, S. D.; Marino, R.; Li, L.; Howarth, R. W.; Alastuey, A.; Alaimo, M. G.; Barraza, F.; Carneiro, M. C.; Chellam, S.; Chen, Y.-C.; Cohen, D. D.; Connelly, D.; Dongarra, G.; Gómez, D.; Hand, J.; Harrison, R. M.; Hopke, P. K.; Hueglin, C.; Kuang, Y.-w.; Lambert, F.; Liang, J.; Losno, R.; Maenhaut, W.; Milando, C.; Monteiro, M. I. C.; Morera-Gómez, Y.; Querol, X.; Rodríguez, S.; Smichowski, P.; Varrica, D.; Xiao, Y.-h.; Xu, Y.; Mahowald, N. M. Anthropogenic Perturbations to the Atmospheric Molybdenum Cycle. *Global Biogeochem. Cycles* **2021**, *35* (2), No. e2020GB006787.
(95) Wong, M. Y.; Mahowald, N. M.; Marino, R.; Williams, E. R.; Chellam, S.; Howarth, R. W. Natural atmospheric deposition of molybdenum: a global model and implications for tropical forests. *Biogeochemistry* **2020**, *149* (2), 159−174.
(96) Hulskotte, J. H. J.; Denier van der Gon, H.; Visschedijk, A. J. H.; Schaap, M. Brake wear from vehicles as an important source of diffuse copper pollution. *Water Sci. Technol.* **2007**, *56* (1), 223−231.
(97) Wang, Y.; Li, S.; Wang, M.; Sun, H.; Mu, Z.; Zhang, L.; Li, Y.; Chen, Q. Source apportionment of environmentally persistent free radicals (EPFRs) in PM2.5 over Xi'an, China. *Sci. Total Environ.* **2019**, *689*, 193−202.
(98) Fang, T.; Kapur, S.; Edwards, K. C.; Hagino, H.; Wingen, L. M.; Perraud, V.; Thomas, A. E.; Bliss, B.; Herman, D. A.; De Vizcaya Ruiz, A.; Kleinman, M. T.; Smith, J. N.; Shiraiwa, M. Aqueous OH Radical Production by Brake Wear Particles. *Environ. Sci. Technol. Lett.* **2024**, *11* (4), 315−322.
(99) Chang-Graham, A. L.; Profeta, L. T. M.; Johnson, T. J.; Yokelson, R. J.; Laskin, A.; Laskin, J. Case Study of Water-Soluble Metal Containing Organic Constituents of Biomass Burning Aerosol. *Environ. Sci. Technol.* **2011**, *45* (4), 1257−1263.
(100) Yang, Y.; Battaglia, M. A.; Robinson, E. S.; DeCarlo, P. F.; Edwards, K. C.; Fang, T.; Kapur, S.; Shiraiwa, M.; Cesler-Maloney, M.; Simpson, W. R.; Campbell, J. R.; Nenes, A.; Mao, J.; Weber, R. J. Indoor-Outdoor Oxidative Potential of PM2.5 in Wintertime Fairbanks, Alaska: Impact of Air Infiltration and Indoor Activities. *ACS ES&T Air* **2024**, *1* (3), 188−199.
(101) Khachatryan, L.; Dellinger, B. Environmentally Persistent Free Radicals (EPFRs)-2. Are Free Hydroxyl Radicals Generated in Aqueous Solutions? *Environ. Sci. Technol.* **2011**, *45* (21), 9232−9239.
(102) Khachatryan, L.; Vejerano, E.; Lomnicki, S.; Dellinger, B. Environmentally Persistent Free Radicals (EPFRs). 1. Generation of Reactive Oxygen Species in Aqueous Solutions. *Environ. Sci. Technol.* **2011**, *45* (19), 8559−8566.
(103) Tong, H.; Lakey, P. S. J.; Arangio, A. M.; Socorro, J.; Shen, F.; Lucas, K.; Brune, W. H.; Pöschl, U.; Shiraiwa, M. Reactive Oxygen Species Formed by Secondary Organic Aerosols in Water and Surrogate Lung Fluid. *Environ. Sci. Technol.* **2018**, *52* (20), 11642−11651.
(104) Cheng, A.; Chen, X.; Wu, D.; Li, Q. Toxicity Decreases with the Decay of Environmentally Persistent Free Radicals in Particulate Matter from Incomplete Solid Fuel Burning. *Environ. Sci. Technol. Lett.* **2024**, *11* (5), 459−465.
(105) Yang, Y.; Battaglia, M. A.; Mohan, M. K.; Robinson, E. S.; DeCarlo, P. F.; Edwards, K. C.; Fang, T.; Kapur, S.; Shiraiwa, M.; Cesler-Maloney, M.; Simpson, W. R.; Campbell, J. R.; Nenes, A.; Mao, J.; Weber, R. J. Assessing the Oxidative Potential of Outdoor PM2.5 in Wintertime Fairbanks, Alaska. *ACS ES&T Air* **2024**, *1* (3), 175−187.
(106) Fang, T.; Lakey, P. S. J.; Weber, R. J.; Shiraiwa, M. Oxidative Potential of Particulate Matter and Generation of Reactive Oxygen Species in Epithelial Lining Fluid. *Environ. Sci. Technol.* **2019**, *53* (21), 12784−12792.

https://doi.org/10.1021/acs.est.4c01206
Environ. Sci. Technol. 2024, 58, 14293−14305